



# Chemical vapor deposition of TiN on a CoCrFeNi multi-principal element alloy substrate

Katalin Böör<sup>a,\*</sup>, Ren Qiu<sup>b</sup>, Axel Forslund<sup>c</sup>, Olof Bäcke<sup>b</sup>, Henrik Larsson<sup>c</sup>, Erik Lindahl<sup>d</sup>, Mats Halvarsson<sup>b</sup>, Mats Boman<sup>a</sup>, Linus von Fieandt<sup>d</sup>

<sup>a</sup> Department of Chemistry, Uppsala University, SE-75120 Uppsala, Sweden

<sup>b</sup> Department of Physics, Chalmers University of Technology, SE-41296 Gothenburg, Sweden

<sup>c</sup> Department of Materials Science and Engineering, Royal Institute of Technology, SE-10044 Stockholm, Sweden

<sup>d</sup> AB Sandvik Coromant, SE-12679 Hägersten, Sweden

## ARTICLE INFO

### Keywords:

Chemical vapor deposition  
Transmission electron microscopy  
X-ray diffraction  
Calphad  
Titanium nitride  
Multi-principal element alloy

## ABSTRACT

The reactivity of a quaternary multi-principal element alloy (MPEA), CoCrFeNi, as a substrate in thermal halide chemical vapor deposition (CVD) processes for titanium nitride (TiN) coatings was studied. The coatings were deposited at 850 °C–950 °C using TiCl<sub>4</sub>, H<sub>2</sub> and N<sub>2</sub> precursors. The coating microstructures were characterized using X-ray diffraction (XRD), scanning and transmission electron microscopy (SEM/TEM) with energy dispersive X-ray spectroscopy (EDS). Thermodynamic calculations of substrate and coating stability for a gas phase environment of N<sub>2</sub> and H<sub>2</sub> within a temperature range relevant for the experiments showed that Cr is expected to form hexagonal Cr<sub>2</sub>N and cubic (Ti<sub>1–*e*1</sub>Cr<sub>*e*1</sub>)N or (Cr<sub>1–*e*2</sub>Ti<sub>*e*2</sub>)N phases. These phases could however not be discerned in the samples by XRD after the depositions. Cr was detected at the grain boundaries and the top surface by EDS for a sample synthesized at 950 °C. Grain boundary and surface diffusion, respectively, were the suggested mechanisms for Cr transport into the coating and onto the top surface. Although thermodynamic calculations indicated that Cr is the most easily etched component of the CoCrFeNi alloy to form gaseous chlorides in similar concentrations to that of the residual Ti-chlorides, no sign of etching were found according to the imaging of the sample cross-sections using SEM and TEM. Cross-section and top surface images further confirmed that the choice of substrate had no significant detrimental influence on the film growth or microstructure.

## 1. Introduction

Multi-principal element alloys (MPEAs) have been widely studied since 2004 [1–3]. These alloys comprise several elements in near-equiatomic ratios, making none of the elements a main component as in traditional alloys. In the literature, the name high-entropy alloys (HEAs) is commonly used, which is correct only if the stabilizing factor is the high configurational entropy [4,5].

The current study focuses on the possibility of coating CoCrFeNi — the base alloy of the most widely studied MPEA family [3] — with TiN in a chemical vapor deposition (CVD) process. The substrate constituent elements are the main components of stainless steel and nickel-rich alloys, accentuating the practical importance of the alloy. Superior corrosion, oxidation and mechanical impact resistance of conventional alloys is often achieved by depositing protective coatings, probably being indispensable for new materials as well. TiN is a well-established coating for biomedical applications (e.g. orthopedic implants, neural

electrodes) and for cutting tools [6–8]. Protective coatings can be synthesized by various methods including physical vapor deposition (PVD) and CVD, where the latter is essential for the coating of materials of complex shapes and allows higher growth rates.

The current investigation is a stability study of the substrate, the coating and the TiN deposition precursors under the process conditions. The substrate was coated by TiN using TiCl<sub>4</sub>, N<sub>2</sub> and H<sub>2</sub> precursors at three different temperatures. The stability of the coexisting TiN-CoCrFeNi phases as well as that of the CoCrFeNi phase in the presence of the precursors were investigated. Where phases other than the desired TiN and CoCrFeNi were observed or predicted by thermodynamic calculations, the mechanisms governing their formation were studied, including diffusion and substrate etching by Cl-containing intermediates followed by re-deposition. It was also investigated if the film crystal growth is disturbed in any way by the substrate in comparison with conventional CVD processes where the substrate only influences nucleation, coalescence and initial growth at the substrate-

\* Corresponding author.

E-mail address: [katalin.boor@kemi.uu.se](mailto:katalin.boor@kemi.uu.se) (K. Böör).

<https://doi.org/10.1016/j.surfcoat.2020.125778>

Received 17 February 2020; Received in revised form 27 March 2020; Accepted 13 April 2020

Available online 21 April 2020

0257-8972/ © 2020 Published by Elsevier B.V.

coating interface.

In previous studies of the MPEA family the thermal stability of the single-phase CoCrFeNi was claimed when heat-treated between 800 °C–1100 °C for 96 h and at 1200 °C for 1 h [9,10]. These studies indicate that CoCrFeNi seems to withstand the temperatures required for CVD syntheses. Corrosion resistance of the substrate is important for halide CVD processes. High corrosion resistance of the CoCrFeNi alloy was reported and attributed to the presence of Cr, which presumably is due to its compact oxide [11]. Furthermore, the CoCrFeNi alloy consists of one single phase, which usually yields better corrosion resistance compared to multi-phase alloys [12–14].

Other studies using TiCl<sub>4</sub> as a precursor for CVD on elemental Co, Fe, Ni substrates and alloys of Co, Cr, Fe and Ni have been carried out [15–17]. An Fe substrate was found to be strongly etched by the TiCl<sub>x</sub> precursor species or the HCl by-product [15]. Higher deposition rates were measured on Ni substrates compared to Co substrates, and an additional crystalline phase forming on Ni was also reported [15,16]. The additional phase was confirmed to be Ni<sub>3</sub>Ti in the former reference and it caused less dense coatings as it formed. Co and Ni were also found in the CVD coatings of TiC on cemented carbides, WC-Co and TiCN-Ni-Mo, Ni having a higher concentration [17]. In the same study, Cr was present in the coating in a substantially higher concentration than Fe compared to their relative contents in a stainless steel substrate. However, in this case it must be taken into account that Cr is more prone to carbide formation than Fe, with a lower standard enthalpy of formation of its carbide [18]. The incorporation of the substrate elements in the CVD coatings were suggested to be caused by either diffusion from the substrate or chlorination-redeposition, the elements first forming gaseous compounds by reacting with Cl and then re-deposited into the coating during the CVD process [15,17]. Fe and Ni substrates perform poorly in CVD of TiN and TiC coatings, which hence raises the question if the substrate stability in CVD syntheses improves by alloying them with equal amounts of Co and Cr to obtain CoCrFeNi as a new substrate material. The question is investigated in detail in this article. In a previous study, a CoCrFeNi-bound cemented carbide could be CVD-coated with Ti(C,N), Al<sub>2</sub>O<sub>3</sub> and TiN without any detrimental effects on the mechanical performance of the coated material, indicating that the alloy could be compatible with halide CVD processes [19].

## 2. Material and methods

### 2.1. Synthesis

The substrate material was prepared by arc melting using pressed pellets of Co (99.3 wt% Co, 0.4 wt% O and 0.1 wt% C) as 1 μm particles, granulated with 2 wt% polyethylene glycol (PEG) used as pressing aid, Ni (99.8 wt%, 0.1 wt% O) as < 26 μm pieces, Fe (99.9 + %, metal basis 99.95%) as < 10 μm particles together with Cr (99.995%) as 2–3 mm pieces. The sample was flipped over and remelted several times for homogenization. Thereafter, the arc melted button was cut in horizontal direction to discs in order to obtain a flat surface. The discs were then heat-treated at 1200 °C under flowing Ar atmosphere for 36 h with the aim to obtain equiaxial grains of the as-cast alloys [9,10]. The samples were ground by a SiC paper with grit number 220 and consecutively polished by diamond paste slurries with particle diameters of 9, 3 and 1 μm. Thereafter the samples were coated using TiCl<sub>4</sub>, H<sub>2</sub> and N<sub>2</sub> precursors in a Bernex 530 s hot wall CVD reactor at three different temperatures ranging from 850 °C to 950 °C. The coating parameters are shown in Table I. The deposition times were chosen to attain coatings of reasonably similar thicknesses ranging from 0.5 to 3 μm. The reactor was left to cool in a nitrogen atmosphere after the depositions.

### 2.2. Characterization

The phase content of the substrate material was analyzed by a

**Table I**  
CVD synthesis parameters.

T [°C]	H <sub>2</sub> [mbar]	N <sub>2</sub> [mbar]	TiCl <sub>4</sub> [mbar]	P <sub>total</sub> [mbar]	Deposition time [h]
850	195	195	10	400	6.0
900	195	195	10	400	5.5
950	195	195	10	400	5.0

Bruker D8 Advance X-ray diffraction instrument, equipped with LynxEye XE-T detector with high energy resolution, thereby filtering out most of the X-ray fluorescence disturbance from the substrate elements. Cu Kα radiation was used in all the diffraction studies. GI-XRD was carried out for discerning the crystalline phases present in the coatings using a Philips MRD-XPRT diffractometer. The instrument was equipped with an X-ray mirror at the incident beam side with a mirror slit yielding a full beam of 1.4 mm and a 0.04 rad sollar slit. A 0.27° collimator was placed in front of the proportional detector. The incident angle was set to 2°. Zeiss field emission gun (FEG) scanning electron microscopes (SEM) were used for characterizing the morphology and the cross-section of the coatings in order to investigate a possible substrate etching or detrimental effects on the film growth. STEM/TEM analyses were performed for detailed cross-sectional characterization. TEM lift-out samples were prepared by a focused ion-beam (FIB) method using a Helios Nanolab FIB-SEM system with an easy-lift micromanipulator. STEM/TEM characterization was performed using an FEI Titan 80-300 TEM/STEM instrument operated at 300 kV. EDS analysis was performed in STEM mode using an Oxford X-sight EDS detector with the aim to map the distribution of substrate components in the coatings and to suggest their transport mechanisms to the coating. The EDS detector is a lithium-doped silicon single-crystal semiconductor (Si(Li)) detector which has an energy resolution of 136 eV at 5.9 keV.

## 3. Calculation

The Thermo-Calc software was used to predict the stable phases as a function of temperature and N (nitrogen) content of the gas phase [20]. Thermo-Calc utilizes the Calphad method to evaluate thermodynamic quantities based on assessed thermodynamic data stored in databases [21]. The Calphad method was first introduced to include all available experimental data of a system and construct a characteristic state function, usually Gibbs energy, for each phase in the system. This state function can then be used to evaluate thermodynamic quantities by minimizing the energy of the system under some appropriate constraints.

The data used for the calculations were taken from the TCFE8 database for the condensed phases and from the SSUB6 database for the gas phase [22,23]. Mainly two sets of calculations were carried out. The first set focused on the condensed phases that were likely to form. In these calculations the mole fractions of the metal species were set to 0.1 and the mole fraction of H (hydrogen) was allowed to vary as a stepping was executed over the N mole fraction. Any pressure dependence was neglected and the pressure was set to 1 × 10<sup>5</sup> Pa. In addition, a calculation was performed with only Ni as the substrate, but with all other conditions kept unchanged. The second set of calculations was carried out to analyze the possibility of substrate etching by the gas phase species. Therefore, here Cl (chlorine) was also included. In the calculation with Cl the relative amounts of Cl, H and N were set to be the same as in the experiments, as specified in Table I.

All relevant phases in the databases were included in the calculations, including the ones predicted to be stable close to the gas conditions in the experiments: the cubic close-packed solid solution of Co, Cr, Fe and Ni (CoCrFeNi), the gas phase, the hexagonal Cr<sub>2</sub>N (h-Cr<sub>2</sub>N) and the cubic Ti- and Cr-nitrides. The Ti/Cr-nitrides are in the TCFE8

database modeled as a single phase with a miscibility gap, with its maximum at around 900 °C. The composition sets at each side of the miscibility gap are in this work labeled as  $(\text{Ti}_{1-\varepsilon_1}\text{Cr}_{\varepsilon_1})\text{N}$  and  $(\text{Cr}_{1-\varepsilon_2}\text{Ti}_{\varepsilon_2})\text{N}$ , respectively, with the subscript '1 -  $\varepsilon$ ' indicating the main component on the metal sublattice. The label  $(\text{Ti,Cr})\text{N}$  is used for regions completely outside the miscibility gap where the relative Ti/Cr occupation on the metal sites may vary in the whole composition range without any phase separation. Additionally, the non-stoichiometry on the N site was for simplicity not indicated throughout this work, even though the Calphad models used include N deficiencies.

Calculations were made for varying N content, with the H content set as a dependent variable. In these calculations the relative amounts of gas phase compared to solid phases have been set relatively high. Only for very small gas contents will the amount of N in the gas be so small that the formation of  $\text{Cr}_x\text{N}$  would influence the gas N concentration to differ from the experimental N gas concentration and subsequently alter the N activity and affect the calculation results. Such small gas contents were not taken into account here, since the experiments are carried out with high excess of N in the gas phase.

## 4. Results and discussion

### 4.1. Thermodynamic calculation results

In Fig. 1 the condensed phases predicted to be stable are shown in detail as a function of temperature and H/N ratio in the gas. Note that the nitrogen activity increases to the left; to lower H/N ratios. Based on a prior study, an additional condensed phase —  $\text{Ni}_3\text{Ti}$  — could be expected in the presence of Ti and Ni [15]. There, the  $\text{Ni}_3\text{Ti}$  phase was shown to cause disturbances in the TiN film growth on pure Ni substrates, although thermodynamic calculations did not predict its presence. In that paper, it was further proposed that the  $\text{Ni}_3\text{Ti}$  phase formed since Ti-containing precursors and intermediates were more reactive than those containing nitrogen. In the present study, having Co, Cr, Fe and Ni in equal concentrations,  $\text{Ni}_3\text{Ti}$  is only stable at very low N activity (corresponding to around  $10^{-11}$  volume fraction  $\text{N}_2$  in the gas phase) as opposed to our corresponding thermodynamic calculations with a Ni substrate, where Ni is more prone to form  $\text{Ni}_3\text{Ti}$ , for volume fractions of  $\text{N}_2$  more than two orders of magnitude higher. This indicates that the multicomponent substrate would be less reactive than pure Ni. Furthermore, the calculations predict that the CoCrFeNi phase should be present at equilibrium, coexisting with the gas. As the N mole

fraction in the gas increases, the CoCrFeNi phase gets depleted of Cr which forms  $\text{Cr}_x\text{N}$  and solid solution nitrides with Ti. Therefore, Cr is predicted to diffuse most probably into the coating if any diffusion in connection with N- and Ti-activities occurs. The above thermodynamic analysis does not consider any kinetics of the systems. Reaction kinetics does influence, and may completely govern, growth processes. However, the driving forces are determined by the thermodynamics which is a helpful tool in analyzing reaction processes.

In Fig. 1a), the TiN phase coexists with the cubic CrN phase at lower temperatures, with some solubility of Ti and Cr as  $(\text{Ti}_{1-\varepsilon_1}\text{Cr}_{\varepsilon_1})\text{N}$  and  $(\text{Cr}_{1-\varepsilon_2}\text{Ti}_{\varepsilon_2})\text{N}$ , respectively. In the TCFE8 database the top of the miscibility gap is estimated to fall slightly above 800 °C, above which the solubility allows the formation of one common nitride.

To clearer see the effect of gas N concentration on the formation of  $\text{Cr}_x\text{N}$  from the CoCrFeNi substrate, an additional diagram from calculations with Ti absent is shown in Fig. 1b) to survey the possible  $\text{Cr}_x\text{N}$  phases. The first  $\text{Cr}_x\text{N}$  phase that is predicted to form at low to intermediate temperatures is hexagonal  $\text{Cr}_2\text{N}$ , which at higher N activities transforms into cubic NaCl-type structured CrN. With rising temperature the chromium shows an increased tendency to reside in the CoCrFeNi phase, rather than form a nitride.  $\text{Cr}_2\text{N}$  is also stable at higher temperatures than CrN.

The reactivity of the substrate towards Cl-containing species has also been evaluated. Thermodynamic calculations performed predict that  $\text{CrCl}_3$  is among the most stable metal chlorides in the gas phase in the presence of the CoCrFeNi substrate and TiN. The relative ratios of the respective sums of various Cr, Fe and Ti chlorides in the gas phase can be seen in Fig. 2 in a temperature range covering the deposition conditions in this work. There are two Cr-chlorides present,  $\text{CrCl}_3$  and  $\text{CrCl}_2$ , that contribute to the Cr-chlorides ratio in the figure.  $\text{CrCl}_2$  presents a non-negligible fraction only above around 875 °C. The  $\text{CrCl}_3$  becomes the most stable chloride just above 800 °C. At the high temperatures applied experimentally (above 850 °C) the Cr-chlorides are the most stable ones compared with the other chlorides. This suggests that from a thermodynamic perspective, the largest risk for metal depletion by etching is carried by Cr during the coating process.

### 4.2. Phase analysis

The X-ray diffractogram of the substrate material recorded after the polishing step (Fig. 3a)) indicated that the substrate is single-phase [24] as previously described in the literature [10]. A logarithmic scale was

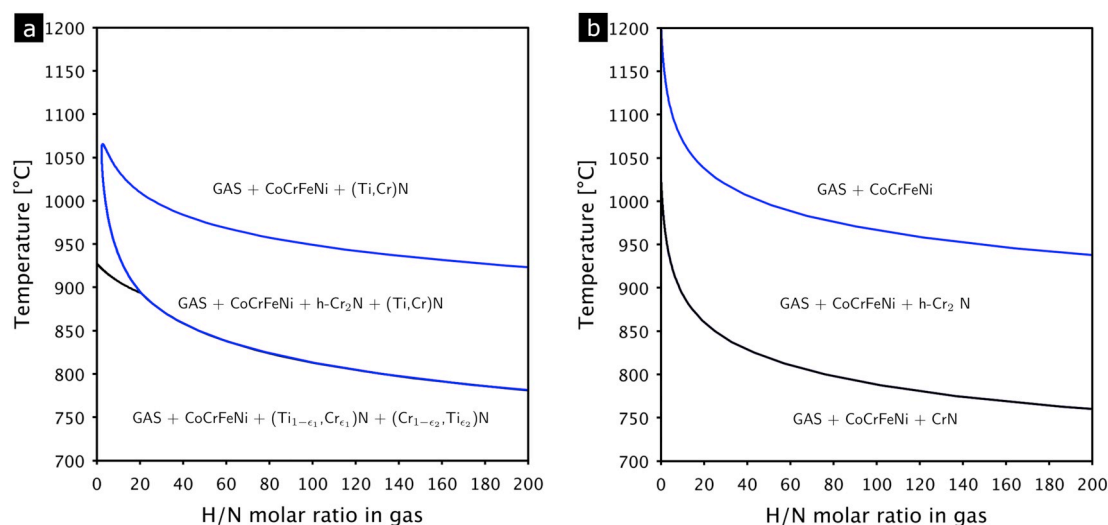


Fig. 1. Isoleths as a function of temperature (in °C) and the H/N molar ratio in the gas phase. All phases have been marked in the plots, including the multicomponent CoCrFeNi solid solution; the gas phase, the Ti rich  $(\text{Ti}_{1-\varepsilon_1}\text{Cr}_{\varepsilon_1})\text{N}$ ; the Cr rich  $(\text{Cr}_{1-\varepsilon_2}\text{Ti}_{\varepsilon_2})\text{N}$ ; a high temperature solution of  $(\text{Ti,Cr})\text{N}$ , stable at its whole Ti-Cr composition range; and a hexagonal  $\text{Cr}_2\text{N}$ . The calculations include the elements of the substrate in the presence of (a) Ti and N and (b) only N.

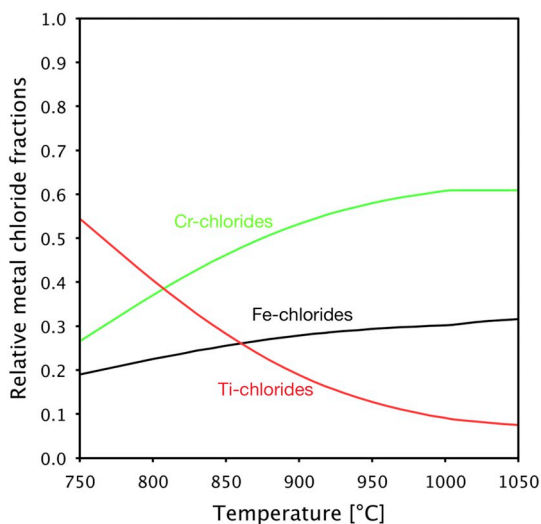


Fig. 2. Relative ratios of the respective sums of the Cr, Fe and Ti chlorides in the gas phase as function of temperature.

applied to the y-axis (intensity) to enhance the visibility of minor peaks. The substrate was strongly {100} textured with respect to the direction of cooling after arc melting. The indicated additional peaks are a result of Cu  $K\alpha_2$ , Cu  $K\beta$  and W  $L\alpha_{1,2}$  radiation contamination, which appear with a detectable intensity due to the strong {100} texture. The peaks resulting from the radiation contamination are shown in Fig. 3(a)) at their expected positions. The GI-XRD measurements carried out after the depositions (Fig. 3b)) show that TiN [25] was formed on the substrates at all the applied temperatures. Apart from the TiN peaks, substrate peaks [24] could be observed. Due to the peak overlaps at other positions, a peak around  $2\theta = 46.5^\circ$  would be a fingerprint position of the  $Ni_3Ti$  phase [26], but was not found; in agreement with the expectations from the thermodynamic calculations to be observable only at extremely low nitrogen activity (corresponding to around  $10^{-11}$  volume fraction  $N_2$  in the gas phase). Patterns of hexagonal or cubic chromium nitride phases were not found in the diffractograms. The peaks of the cubic nitride phase would appear at slightly higher angles than those of the TiN phase, if occurring in a two-phase mixture. Cr is slightly soluble in the TiN phase, which instead could result in peak shifts or, if there are concentration gradients of the solution over the grains, apparently asymmetric peaks. Such features were not observed in the diffractograms. According to the XRD results, the substrate material is inert towards Cr depletion under the applied reaction conditions, since only TiN, CoCrFeNi and no other crystalline phases were discerned in the GI-diffractograms.

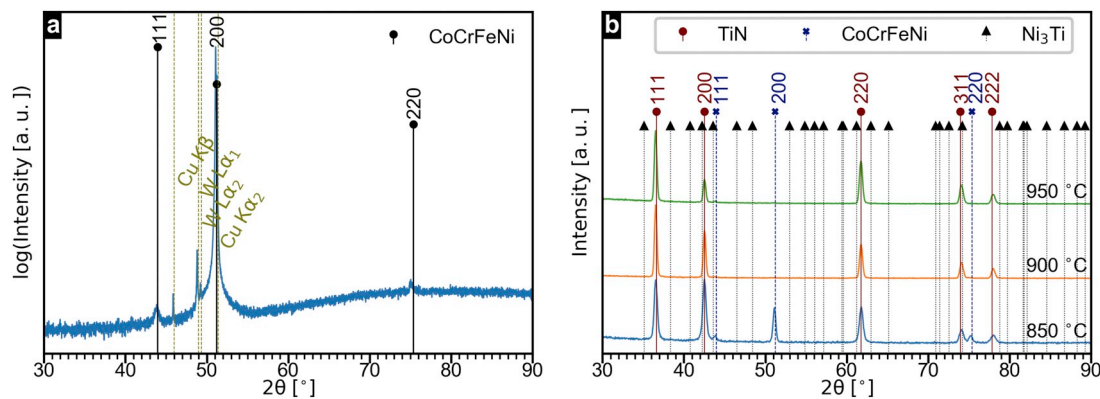


Fig. 3. (a) X-ray diffraction pattern of the substrate material (reference pattern: [24], ICDD: 04-018-7506). (b) Room temperature grazing incidence X-ray diffraction patterns of the samples synthesized at different temperatures (reference patterns: CoCrFeNi: [24], ICDD: 04-018-7506; TiN: [25], ICDD: 04-016-3390, the cell parameter has been tuned by 1.004 in the figure;  $Ni_3Ti$ : [26], ICDD: 04-016-3390).

### 4.3. Coating microstructures

The SEM images (Fig. 4) indicate different surface morphologies and thus different growth on changing the temperatures. At 850 °C the grains are more needle-like from the top view (with a length of a couple of hundred nanometers to one micrometer in one dimension). At higher temperatures the grains are faceted on the top surface, with a diameter of 0.5–1.5  $\mu m$ , where measurable. Previous results have shown that the coating temperature influences the film microstructure [27–29]. The star-shaped grains with a five-fold symmetry, appearing in all three coatings, are commonly seen for TiN coatings [29,30]. No sign of growth disturbance caused by the substrate were observed from the top surface, as opposed to the situation for elemental Fe and Ni substrates, where the effect was clear in the top view images [15]. The cross-section images do not show any severe etching of, or reaction with the substrate, as opposed to what has previously been observed for the elemental Fe or Ni substrates [15]. Small voids (10–90 nm in diameter) can be seen at the substrate-coating interface of the sample synthesized at 850 °C (Fig. 4d)). The voids are probably not a result of substrate etching, since the surface roughness of the three substrates is similar and is inherited from the polishing process. The voids in the coating may probably be attributed to slow surface diffusion in relation to the grain growth in the surface-normal direction at 850 °C, whereas this is not the case for the other two, higher deposition temperatures.

Fig. 5 shows TEM bright field (BF) and STEM high-angle annular dark field (HAADF) micrographs collected from the sample coated at 950 °C. Fig. 5(a) and b) show the grain morphology close to the substrate/coating interface, where round TiN grains have formed. No severe etching of the substrate can be seen, although the substrate was expected to be most reactive towards the gas phase at 950 °C, the highest temperature of this study. As shown in Fig. 5(c), columnar grains of 1.5–2.5  $\mu m$  in length start to form about 1  $\mu m$  from the substrate-coating interface. This kind of grain growth (zone T growth) is present when the ratio between the substrate temperature ( $T_s$ ) and the melting temperature of the coating ( $T_m$ ) — both expressed in K — fall in the approximate range of  $0.2 < T_s/T_m < 0.4$  [31,32]. At the initial stage of the coating process, nuclei form, which grow into islands and consecutively coalesce into round grains, as also indicated in Fig. 5. Further on, the deposition temperature is high enough ( $T_s/T_m > 0.2$ ) to enable adatom diffusion on the top surface and epitaxial growth with respect to each underlying grain surface. On those surface planes where the adatoms experience lower diffusivity, they will reside longer and thus will have a higher probability to be incorporated in the grains of those. In a competitive way, the mentioned grains grow in a columnar manner, at a higher rate compared with grains with other orientations. The temperature is too low ( $T_s/T_m < 0.4$ ) to allow for bulk diffusion of the coating, which would result in re-crystallization into large,

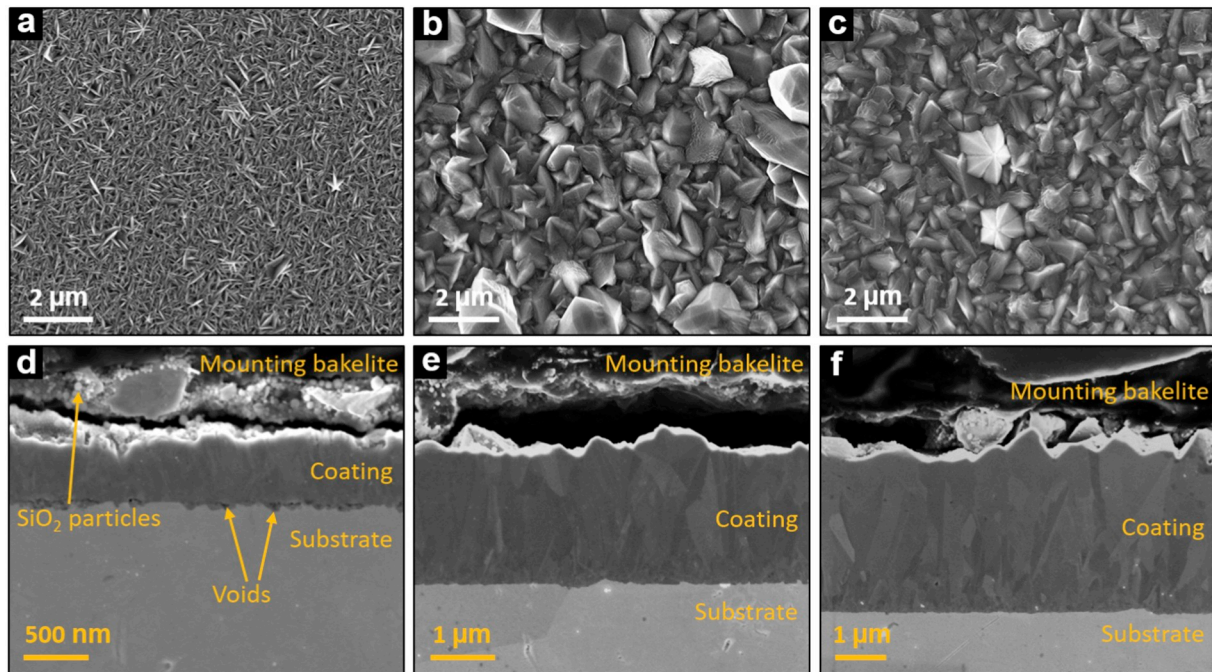


Fig. 4. SEM secondary electron (SE) images of the top surfaces and cross-sections of the coatings deposited at (a), (d) 850 °C; (b), (e) 900 °C; and (c), (f) 950 °C. The mounting resin of bakelite, the coating, the substrate, the SiO<sub>2</sub> particles from the polishing slurry and the voids in the coating are marked in the cross-section micrographs.

thermodynamically stable grains. (For a more detailed description of the zone model the reader is referred to the references [31, 32]. The coating microstructure resembles that of conventional coatings, where the substrate only influences nucleation, island growth, coalescence and grain growth at the substrate-coating interface and further growth is governed by the reaction parameters.

Fig. 6 shows the analytical STEM results of the coating deposited at 950 °C. The STEM HAADF micrograph (Fig. 6a) illustrates the distribution of the round nitride grains close to the substrate. The STEM EDS mapping reveals that Cr is present within the TiN coating, concentrated along the grain boundaries, as shown in the insert of Fig. 6a). The other elements of the substrate alloy could not be detected. Fig. 6b) shows a sample detail with a grain boundary, where data from an EDS line-scan were collected across the boundary, as indicated by the arrow. In Fig. 6c) the concentration profiles of the substrate elements are presented as a percentage of the total metallic element content. Cr is found to exhibit an aggregation of around 1.5 at.% at the grain boundary. Fig. 6d) shows the top surface of the TiN coating where an EDS line-scan was acquired along the surface normal as indicated by the

arrow. In Fig. 6e) Cr is found aggregated at the coating top surface, around 1 at.%. However, the content of Cr determined by EDS might be lower than the actual value considering the beam-broadening effect. Diffusion would be expected to result in a negative concentration gradient of Cr towards the surface.

The findings from the EDS measurements correlate with the thermodynamic calculations, indicating that Cr would form (Ti<sub>1-ε<sub>1</sub></sub>Cr<sub>ε<sub>1</sub></sub>)N. The minute amounts found in the EDS measurements explain the absence of Cr<sub>2</sub>N or Ti<sub>1-ε<sub>1</sub></sub>Cr<sub>ε<sub>1</sub></sub>N/Cr<sub>1-ε<sub>2</sub></sub>Ti<sub>ε<sub>2</sub></sub>N peaks in the GI-XRD. We suggest that the Cr enrichment in the top part of the coating could be explained by the cooling conditions, where the N-rich cooling atmosphere could enhance the accumulation of Cr on the surface of the coating through continued diffusion during the cooling stage. Another gradient could be expected close to the coating top surface, with increasing Cr content towards the top surface. This could be the result of Cr<sub>x</sub>N formation on the surface being energetically favorable. The grain boundaries close to the surface could be depleted of Cr if the supply to replace Cr from the substrate by grain boundary diffusion is slower than the depletion by diffusion on the surface. The minute concentrations

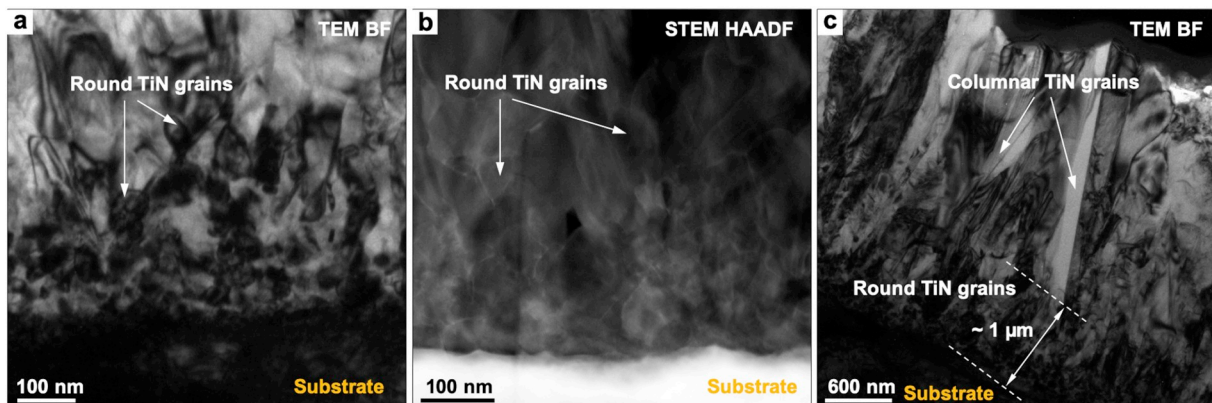
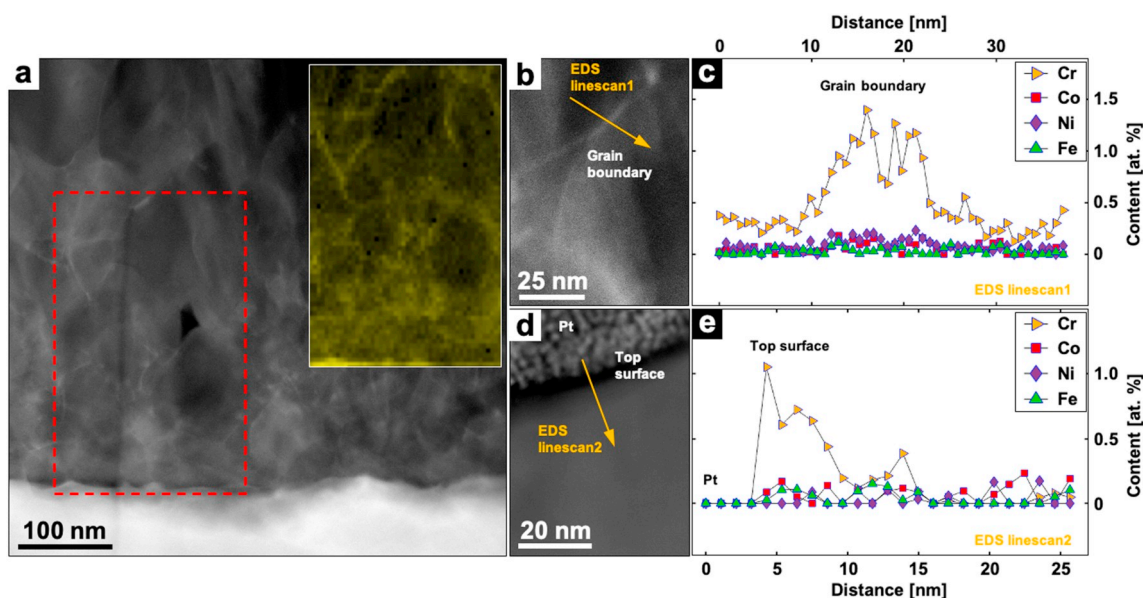


Fig. 5. Grain morphology variation of the coating deposited at 950 °C disclosed by (S)TEM. (a) and (b) are, respectively, TEM BF and STEM HAADF micrographs acquired in the vicinity of the TiN/CoCrFeNi-substrate interface and (c) is a TEM BF image of the whole coating cross-section.



**Fig. 6.** Analytical STEM results of the sample coated at 950 °C. (a) STEM HAADF micrograph of the coating cross-section with EDS mapping of Cr from the dashed marked area inserted at the top right corner. (b) and (d) are STEM HAADF micrographs showing, respectively, a TiN grain boundary and the TiN coating top surface. (c) and (e) are EDS linescan profiles collected from a grain boundary and the coating top surface, respectively, as indicated in (b) and (d).

and thus the minute variations in concentrations, however, do not allow for an exact determination of the mentioned gradients.

Since no apparent etching could be observed either by SEM or TEM, the etching of Cr to form  $\text{CrCl}_x$  species and being followed by  $\text{Cr}_x\text{N}$  deposition from the chlorides is most likely negligible. The statement is further supported by the Cr enrichment in the grain boundaries: etching and re-deposition of Cr would namely yield a homogeneous Cr distribution within the grains. Cr would be mainly present at the substrate-coating interface, with a gradually decreasing concentration towards the top surface. The substrate depletion of Cr and its segregation in the grain boundaries are suggested to be caused by diffusion, being most prominent there as well as on the surface due to the higher concentration of defects and weaker bonding. The diffusion of Cr is most likely driven by the high N-activity at the surface, both during deposition and cooling.

## 5. Conclusions

Characterization of TiN coatings deposited by CVD on CoCrFeNi MPEA substrates at 850 °C–950 °C using  $\text{TiCl}_4$ ,  $\text{H}_2$  and  $\text{N}_2$  precursors gave the following results on coating structure, substrate reactivity and substrate/coating thermodynamic stability:

- Cr- and Ti/Cr-nitrides were predicted by thermodynamic calculations. Cr appeared in the grain boundaries of the coating deposited at 950 °C and on its top surface, as shown by STEM EDS.
- Cr was expected to be etched most easily of all the substrate elements, based on its relatively larger abundance in the form of gas-phase chlorides under the coating process conditions, as predicted by thermodynamic calculations. However, SEM/TEM imaging did not show any significant etching at the substrate-coating interface.
- Grain boundary diffusion during the coating process and surface diffusion upon cooling in  $\text{N}_2$  are the most probable mechanisms of Cr transport from the substrate, deduced from the above stated results.
- No  $\text{Ni}_3\text{Ti}$  phase was formed as opposed to the case of depositions on pure Ni [15]. The result was predicted by thermodynamic calculations and corroborated experimentally by GI-XRD and EDS in STEM.
- The coating deposited at 950 °C was built up by equiaxial grains up to 1  $\mu\text{m}$  thickness followed by columnar grains. This coating

microstructure is a result of competitive grain growth, typical of the deposition temperature for this coating material (zone T growth [31,32]). The substrate did not disturb the expected growth.

- Apart from the slight depletion of Cr, the substrate remained intact during the coating processes.

The current study contributes to the detailed investigation of the MPEA family based on Co, Cr, Fe and Ni by shedding light on the low reactivity of the CoCrFeNi base alloy in a surface treatment process involving halogen compounds and temperatures between 850 and 950 °C.

## CrediT authorship contribution statement

**Katalin Bőör:** Investigation, Formal analysis, Visualization, Writing - original draft. **Ren Qiu:** Investigation, Formal analysis, Visualization, Writing - original draft. **Axel Forslund:** Investigation, Formal analysis, Visualization, Writing - original draft. **Olof Bäcke:** Supervision, Writing - review & editing. **Henrik Larsson:** Funding acquisition, Supervision, Writing - review & editing. **Erik Lindahl:** Supervision, Writing - review & editing. **Mats Halvarsson:** Funding acquisition, Supervision, Writing - review & editing. **Mats Boman:** Funding acquisition, Project administration, Supervision, Writing - review & editing. **Linus von Fieandt:** Conceptualization, Investigation, Resources, Supervision, Writing - review & editing.

## Declaration of competing interest

The authors declare that they have no known competing financial interests or personal relationships that could have appeared to influence the work reported in this paper.

## Acknowledgement

Funding from the Swedish Foundation for Strategic Research via SSF contract RMA15-0048 and AB Sandvik Coromant is gratefully acknowledged. The transmission electron microscopy experiments were carried out at the Chalmers Materials Analysis Laboratory (CMAL), Gothenburg. Rolf Berger is also acknowledged for the linguistic correction of the article.

## References

- [1] B. Cantor, I.T. Chang, P. Knight, A.J. Vincent, Microstructural development in equiatomic multicomponent alloys, *Mater. Sci. Eng. A* 375–377 (2004) 213–218, <https://doi.org/10.1016/j.msea.2003.10.257>.
- [2] J.-W. Yeh, et al., Formation of simple crystal structures in Cu-Co-Ni-Cr-Al-Fe-Ti-V alloys with multiprincipal metallic elements, *Metall. Mater. Trans. A* 35A (2004) 2533–2536, <https://doi.org/10.1007/s11661-006-0234-4>.
- [3] J.W. Yeh, et al., Nanostructured high-entropy alloys with multiple principal elements: Novel alloy design concepts and outcomes, *Adv. Eng. Mater.* 6 (2004) 299–303, <https://doi.org/10.1002/adem.200300567>.
- [4] D.B. Miracle, O.N. Senkov, A critical review of high entropy alloys and related concepts, *Acta Mater.* 122 (2017) 448–511, <https://doi.org/10.1016/j.actamat.2016.08.081>.
- [5] B.E. MacDonald, et al., Recent Progress in High Entropy Alloy Research, *JOM* 69 (2017) 2024–2031, <https://doi.org/10.1007/s11837-017-2484-6>.
- [6] K. Bobzin, High-performance coatings for cutting tools, *CIRP J. Manuf. Sci. Technol.* 18 (2017) 1–9, <https://doi.org/10.1016/j.cirpj.2016.11.004>.
- [7] R.P. van Hove, I.N. Siersevelt, B.J. van Royen, P.A. Nolte, Titanium-Nitride Coating of Orthopaedic Implants: A Review of the Literature, *Biomed. Res. Int.* 2015 (2015) 1–9, <https://doi.org/10.1155/2015/485975>.
- [8] C. Outen, D. Konopka, T. Fennessey, Development of Titanium Nitride Fractal Coatings for Cardiac and Neural Electrostimulation Electrodes, *Society of Vacuum Coaters 57th (2014) Annual Technical Conference Proceedings*, 57 (2014), pp. 33–37, <https://doi.org/10.14332/svc14.proc.1819>.
- [9] M. Vaidya, K. Guruvadyathri, B.S. Murty, Phase formation and thermal stability of CoCrFeNi and CoCrFeMnNi equiatomic high entropy alloys, *J. Alloys Compd.* 774 (2019) 856–864, <https://doi.org/10.1016/j.jallcom.2018.09.342>.
- [10] Z. Wu, H. Bei, F. Otto, G.M. Pharr, E.P. George, Recovery, recrystallization, grain growth and phase stability of a family of FCC-structured multi-component equiatomic solid solution alloys, *Intermetallics* 46 (2014) 131–140, <https://doi.org/10.1016/j.intermet.2013.10.024>.
- [11] X.L. Shang, Z.J. Wang, F. He, J.C. Wang, J.J. Li, J.K. Yu, The intrinsic mechanism of corrosion resistance for FCC high entropy alloys, *Sci. China Technol. Sci.* 61 (2018) 189–196, <https://doi.org/10.1007/s11431-017-9114-1>.
- [12] Y.J. Hsu, W.C. Chiang, J.K. Wu, Corrosion behavior of FeCoNiCrCu<sub>x</sub> high-entropy alloys in 3.5% sodium chloride solution, *Mater. Chem. Phys.* 92 (2005) 112–117, <https://doi.org/10.1016/j.matchemphys.2005.01.001>.
- [13] Y.F. Kao, T.D. Lee, S.K. Chen, Y.S. Chang, Electrochemical passive properties of Al<sub>x</sub>CoCrFeNi (x = 0, 0.25, 0.50, 1.00) alloys in sulfuric acids, *Corrosion Sci.* 52 (2010) 1026–1034, <https://doi.org/10.1016/j.corsci.2009.11.028>.
- [14] C.M. Lin, H.L. Tsai, Evolution of microstructure, hardness, and corrosion properties of high-entropy Al<sub>0.5</sub>CoCrFeNi alloy, *Intermetallics* 19 (2011) 288–294, <https://doi.org/10.1016/j.intermet.2010.10.008>.
- [15] L. von Fieandt, T. Larsson, E. Lindahl, O. Bäcke, M. Boman, Chemical vapor deposition of TiN on transition metal substrates, *Surf. Coat. Technol.* 334 (2017) 373–383, <https://doi.org/10.1016/j.surfcoat.2017.11.063>.
- [16] J.C. Nable, S. Nosheen, S.L. Suib, F.S. Galasso, Atmospheric pressure chemical vapor deposition of titanium nitride on metals, *Surf. Coat. Technol.* 200 (2006) 2821–2826, <https://doi.org/10.1016/j.surfcoat.2005.02.171>.
- [17] I.Y. Konyashin, The influence of Fe-group metals on the CVD of titanium carbide, *Chem. Vap. Depos.* 2 (1996) 199–208, <https://doi.org/10.1002/cvde.19960020509>.
- [18] S.V. Meschel, O.J. Kleppa, Standard enthalpies of formation of some 3d transition metal carbides by high temperature reaction calorimetry, *J. Alloys Compd.* 257 (1997) 227–233, [https://doi.org/10.1016/S0925-8388\(97\)00023-6](https://doi.org/10.1016/S0925-8388(97)00023-6).
- [19] E. Holmström, et al., High entropy alloys: substituting for cobalt in cutting edge technology, *Appl. Mater. Today* 12 (2018) 322–329, <https://doi.org/10.1016/j.apmt.2018.07.001>.
- [20] J.-O. Andersson, T. Helander, L. Höglund, P. Shi, B. Sundman, THERMO-CALC & DICTRA, computational tools for materials science, *Calphad* 26 (2002) 273–312 URL <http://www.thermocalc.se/>.
- [21] H. Lukas, S.G. Fries, B. Sundman, *Computational Thermodynamics: The Calphad Method*, 1st, Cambridge University Press, New York, NY, USA, 2007.
- [22] Thermo-Calc Software, TCS Steel and Fe-alloys Database version 8.0.
- [23] Thermo-Calc Software, SGTE Substances Database version 6.0.
- [24] M.S. Lucas, et al., Magnetic and vibrational properties of high-entropy alloys, *J. Appl. Phys.* 109 (2011) 1–3, <https://doi.org/10.1063/1.3538936>.
- [25] A.E. van Arkel, *Kristalbouw en physische eigenschappen, Physica (The Hague)* 4 (1924) 286–301.
- [26] F. Laves, H.J. Wallbaum, Die Kristallstruktur von Ni<sub>3</sub>Ti und Si<sub>2</sub>Ti (zwei neue Typen), *Z. Kristallographie* 101 (1939) 78–93, <https://doi.org/10.1524/zkri.1939.101.1.78>.
- [27] H.E. Cheng, M.H. Hon, Texture formation in titanium nitride films prepared by chemical vapor deposition, *J. Appl. Phys.* 79 (1996) 8047–8053, <https://doi.org/10.1063/1.362358>.
- [28] H.E. Cheng, Y.W. Wen, Correlation between process parameters, microstructure and hardness of titanium nitride films by chemical vapor deposition, *Surf. Coat. Technol.* 179 (2004) 103–109, [https://doi.org/10.1016/S0257-8972\(03\)00789-8](https://doi.org/10.1016/S0257-8972(03)00789-8).
- [29] J. Wagner, et al., The effect of deposition temperature on microstructure and properties of thermal CVD TiN coatings, *Int. J. Refractory Met. Hard Mater.* 26 (2008) 120–126, <https://doi.org/10.1016/j.ijrmhm.2007.01.010>.
- [30] H.E. Cheng, M.H. Hon, Growth mechanism of star-shaped TiN crystals, *J. Cryst. Growth* 142 (1994) 117–123, [https://doi.org/10.1016/0022-0248\(94\)90277-1](https://doi.org/10.1016/0022-0248(94)90277-1).
- [31] P.B. Barna, M. Adamik, Fundamental structure forming phenomena of polycrystalline films and the structure zone models, *Thin Solid Films* 317 (1998) 27–33, [https://doi.org/10.1016/S0040-6090\(97\)00503-8](https://doi.org/10.1016/S0040-6090(97)00503-8).
- [32] I. Petrov, P.B. Barna, L. Hultman, J.E. Greene, Microstructural evolution during film growth, *J. Vac. Sci. Technol. A: Vac., Surf., Films* 21 (2003) 117–128, <https://doi.org/10.1116/1.1601610>.